Optical Engineering

OpticalEngineering.SPIEDigitalLibrary.org

OptoNet: a MATLAB-based toolbox for cortical network analyses using functional near-infrared spectroscopy

Gihyoun Lee
Ji-Su Park
Young-Jin Jung

SPIE.

Gihyoun Lee, Ji-Su Park, Young-Jin Jung, "OptoNet: a MATLAB-based toolbox for cortical network analyses using functional near-infrared spectroscopy," *Opt. Eng.* **59**(6), 061602 (2019), doi: 10.1117/1.OE.59.6.061602.

OptoNet: a MATLAB-based toolbox for cortical network analyses using functional near-infrared spectroscopy

Gihyoun Lee,[a] Ji-Su Park,[b] and Young-Jin Jung[c,*]
[a]Sungkyunkwan University School of Medicine, Heart Vascular Stroke Institute, Samsung Medical Center, Center for Prevention and Rehabilitation, Department of Physical and Rehabilitation Medicine, Seoul, Republic of Korea
[b]Dongseo University, Advanced Human Resource Development Project Group for Health Care in Aging Friendly Industry, Busan, Republic of Korea
[c]Dongseo University, Department of Radiological Science, Busan, Republic of Korea

Abstract. Functional brain network analysis is important for understanding the causes of neurological disorders and relevant brain mechanisms. Lately, functional near-infrared spectroscopy (fNIRS) yields outputs similar to the blood-oxygen-level-dependent signals of functional magnetic resonance imaging (fMRI), and numerous studies have been conducted on functional connectivity and causality using fMRI and fNIRS. Despite the existence of numerous analysis toolboxes for fNIRS, most of them are difficult to use because they involve numerous steps, coefficients, and related files. In this study, we developed a MATLAB toolbox called OptoNet, to analyze cortical networks in the brain for fNIRS. Given that OptoNet consists of a simple and intuitive graphical user interface, users can readily analyze the cortical networks of the brain for fNIRS signals. To evaluate the efficacy of the developed toolbox, the finger tapping task experiment—extensively used in brain functional activities and causal connectivity studies—was employed. The experiment was performed using the right and left hands, and both hands simultaneously, and the consequently elicited brain cortical network activity was analyzed using developed OptoNet. [DOI: 10.1117/1.OE.59.6.061602]

Keywords: hemodynamic signal; brain network analysis; functional connectivity; functional near-infrared spectroscopy; phase synchronization; finger tapping task.

Paper 190919SS received Jul. 8, 2019; accepted for publication Aug. 14, 2019; published online Oct. 8, 2019.

1 Introduction

Functional near-infrared spectroscopy (fNIRS) is a noninvasive method used to measure hemodynamic brain signals based on the absorption of near-infrared (NIR) light with wavelengths in the range of 650 to 950 nm transmitted through the intact skull.[1] fNIRS monitors regional cerebral blood flow variations and estimates oxyhemoglobin (HbO) and deoxyhemoglobin (HbR).[2] The hemodynamic signals of fNIRS are highly correlated to the blood-oxygenation-level-dependent signal outputs in functional magnetic resonance imaging (fMRI).[3] However, fNIRS lacks anatomical information when used to localize brain areas that elicit hemodynamic signals. Additionally, it has poor spatial resolution and limits the penetration depth within brain tissue.[4,5] Despite these disadvantages, fNIRS has several advantages compared to other neuroimaging modalities, such as fMRI, positron emission tomography, electroencephalography (EEG), and magnetoencephalography. fNIRS can be used for various experimental environments because it can be able to be portable compared to fMRI and MEG. Since fNIRS system is based on an optical signal, it is stronger than EEG for electrical noise. Therefore, the important advantages of fNIRS are low cost, portability, and the potential of extending the research to various ecological environments.[6]

Over the past decades, many research groups have conducted extensive studies in the field of fNIRS and developed statistical analyses toolboxes to enhance the fNIRS signal quality based on the general linear model (GLM).[7–12] GLM is one of the most extensively used models that represent data in a linear combination form and constitute a standard method for analyzing the fMRI data. Many statistical analysis toolboxes have been developed for fNIRS based on the GLM.[13–18] However, GLM-based analyses methods often fail to analyze brain functions because of artifacts in the fNIRS measurements. These artifacts exist for various reasons, such as subjects' movements, blood pressure variations, and instrumental instabilities.[19,20] Artifacts cause the fNIRS signal to change abruptly, thereby potentially inducing spikes with amplitudes that are much larger than the true hemodynamic responses. In previous studies, several researchers tried to overcome this problem by using algorithms based on bandpass filtering, moving averaging, and Wiener filtering,[21,22] but these algorithms usually failed to eliminate abrupt noise. Recently, numerous algorithms based on wavelet transform, signal correlation, and artificial neural networks have been adopted for fNIRS signal analysis.[19,22–27] Although these algorithms yield good results, any excess preprocessing leads to attenuation of the hemodynamic response. Therefore, the research interests of fNIRS need to migrate to other analysis methods, such as brain functional connectivity and causality, which are important to achieve a better understanding of brain functions and medical approaches.

Recently, various connections and causality estimation methods for functional brain network analysis have been developed and demonstrated their capacities for utilization in cognitive neuroscience and neurological clinical studies.[28] Correlation,[29,30] coherence,[31] frequency ratio,[32] phase locking value (PLV),[33] mean phase coherence,[34] and mutual

*Address all correspondence to Young-Jin Jung, E-mail: microbme@dongseo.ac.kr

information[35,36] have been used to estimate functional interactions between multiple neural assemblies. These methods have been applied to numerous functional neuroimaging modalities, such as EEG, local field potential, intracranial EEG, MEG, fMRI, and fNIRS. However, there is no available analysis software program of functional brain networks for fNIRS, which can be used for free and unskilled users. The most popular tools currently available for fNIRS analysis are HomER[37] and NIRS–statistical parametric mapping (SPM).[14] HomER (available at Ref. 38) calculates individual hemodynamic responses using ordinary least-squares linear deconvolution, and NIRS–SPM (available at Ref. 39) applies the SPM method, which is a standard activation tool for fMRI for NIRS data. However, these analysis tools cannot estimate functional brain connections and they are difficult to use because of their requirement for various types of information.

The main contribution of the present study is the presentation of a new cortical network analysis toolbox in MATLAB for fNIRS, called "OptoNet," which has an interactive graphical user interface (GUI). OptoNet allows functions to analyze hemodynamic time-series data of fNIRS and also to represent functional connections. Given that OptoNet provides a three-dimensional (3-D) standard head model and various causality estimation methods, the cortical brain network of fNIRS can be clearly identified without any anatomical information and MATLAB scripts. The remainder of this paper introduces the implemented functions of OptoNet and representative experimental examples of the OptoNet toolbox.

2 Theory and Methods

2.1 *fNIRS Measurement Model*

The analyses of functional hemodynamic data, such as fNIRS and fMRI, have generally been based on the assumption of linearity of hemodynamic changes.[40] The modified Beer–Lambert law (MBLL)[2] describes the optical attenuation in scattering media, such as human tissues. Accordingly, the optical density (OD) variation of the HbO and HbR concentration changes (ΔcHbO, ΔcHbR) can be described using the MBLL.[14] According to the MBLL, the raw OD for the wavelength (λ) at the brain cortex position of the 3-D axis at time t is described as follows:[19]

$$\Delta \mathrm{OD}(\lambda_i, r, t) = -\ln\left(\frac{I_\mathrm{m}}{I_0}\right) = \sum_{t=1}^{N_c} a_i(\lambda_i)\Delta c^{(i)}(r,t)d(r)l(r), \tag{1}$$

where I_m denotes the measured optical intensity, I_0 is the initial optical intensity, and N_c is the number of chromophores. Additionally, $a_i(\lambda_i)$ denotes the extinction coefficient at wavelength λ_i of the i'th chromophore, Δc denotes the chromophore concentration changes, $d(r)$ is the differential pathlength factor (DPF),[2] and $l(r)$ is the distance between the sources to the detector at position r. The DPF depends on various parameters, such as the age of the subject[41] and the wavelength of the fNIRS system.[42]

The GLM has been established as a standard analysis model for hemodynamic data from fMRI and fNIRS. SPM has been used extensively within the fMRI domain for hemodynamic functional neuroimages, and there is a MATLAB toolbox for fNIRS called fNIRS SPM.[14] The SPM consists of the model specification, parameter estimation, and statistical inference for hemodynamic data. The corresponding GLM can be transferred to the interpolated measured chromophore concentration changes of HbO and HbR (Δc_HbO and Δc_HbR). The HbO and HbR signals (y_HbO and y_HbR) are described by the following matrix formulation:

$$\begin{bmatrix} y_\mathrm{HbO}(r,t) \\ y_\mathrm{HbR}(r,t) \end{bmatrix} = d(r)l(r)\begin{bmatrix} \Delta c_\mathrm{HbO} \\ \Delta c_\mathrm{HbR} \end{bmatrix} + \begin{bmatrix} \epsilon_\mathrm{HbO}(r,t) \\ \epsilon_\mathrm{HbR}(r,t) \end{bmatrix}, \tag{2}$$

where $\epsilon_\mathrm{HbO}(r,t)$ and $\epsilon_\mathrm{HbR}(r,t)$ are additive zero mean Gaussian noise signals of the fNIRS channels. Let y denote the time series of the hemodynamic signal, and ε be the error vector at location r at time t. The errors (ε) can occur during signal acquisitions from the hair, skull, and pores, and they generally have high-frequency components. The corresponding GLM is represented in the matrix form as follows:

$$\mathbf{y} = [y_\mathrm{HbO}(r,t_1) y_\mathrm{HbO}(r,t_2) \ \cdots \ y_\mathrm{HbO}(r,t_N)]^T, \tag{3}$$

$$\boldsymbol{\varepsilon} = [\varepsilon_\mathrm{HbO}(r,t_1)\varepsilon_\mathrm{HbO}(r,t_2) \ \cdots \ \varepsilon_\mathrm{HbO}(r,t_N)]^T, \tag{4}$$

$$\mathbf{y} = \mathbf{X}\boldsymbol{\beta} + \boldsymbol{\varepsilon}. \tag{5}$$

The elements of $\mathbf{y}$ are the sampled NIRS signal data corresponding to N time points, and $\boldsymbol{\beta}$ represents the unknown strengths of the response. $\mathbf{X}$ is a design matrix that predicts the measured fNIRS signal.[43]

Friston et al.[44] showed that the hemodynamic signal can be approximated as a convolution model between a stimulus function and a hemodynamic response function (HRF). The canonical HRF, which is composed of two gamma functions, was employed in Ref. 16. The derivatives of the HRF with respect to the delay and dispersion can be used to mitigate the problem such that the precise shape of the HRF varies across the brain.[43] An adaptive estimation of HRF using multiple gamma functions can also be used in fNIRS to account for oxygen species-dependent hemodynamic variations.[14]

2.2 *Phase Synchronization-Based Brain Network Estimation Method*

A number of causality estimation techniques have been developed to infer functional interactions between multiple neural assemblies. Lachaux et al.[33] developed a brain network analysis estimator based on phase synchronization (PS) that identifies transient phase-locking between two neuroelectric signals. If the measured fNIRS signal is $x(t)$, the instantaneous phase is constructed by the analytic signal that is defined by the summation of $H(x(t))$ and $x(t)$ as follows:

$$\varphi(t) = \tan^{-1}\frac{(H[x(t)])}{x(t)}, \tag{6}$$

where $\varphi(t)$ are the instantaneous phase, and $H[x(t)]$ is the Hilbert transform of $x(t)$. To estimate the PS between two fNIRS signals [$x_n(t)$ and $x_m(t)$], the phase difference is adopted. The PLV is defined based on the average value of the phase difference as follows:

$$\mathrm{PLV} = \frac{1}{N}\sum_{t=1}^{N} \exp(\varphi_n(t) - \varphi_m(t)), \tag{7}$$

where N is the total sample length of the signal. It estimates the variability of this phase difference between $x_n(t)$ and $x_m(t)$. If the phase difference varies somewhat across the signals, PLV is close to 1; otherwise, it is close to 0.[33]

2.3 *OptoNet: New Cortical Network Analysis Toolbox*

OptoNet requires a MATLAB (MathWorks, Natick, Massachusetts) environment, and it incorporates the MATLAB GUIs that allow users to intuitively analyze the cortical network. The GUI of the toolbox is optimized for MATLAB R2015b and the Nvidia GeForce graphics card series. Figure 1 shows the overall procedure of the OptoNet toolbox. First, the measured fNIRS data are loaded onto the OptoNet GUI. The information of the fNIRS data, such as the sampling rate of the fNIRS signal, task number, size, number of trials, and subject number, are loaded onto the GUI. The fNIRS signal analysis options can control this step before estimating the brain cortical network. OptoNet provides the network analyses options and choices of specific task blocks, or the entire signal lengths for each subject and trial. Second, the head model is loaded onto the GUI to visually represent the fNIRS channels and the brain's causal connectivity.

OptoNet provides a standard head and cortex model and can also support the functionality of loading individual head and cortex models. Third, the channel set of the loaded fNIRS data is represented on the head model. The channel set must be synchronized with the information of the loaded fNIRS channel and the channel set can easily add, save, and load data using the OptoNet GUI. Finally, the brain causal connection of the cortical network is estimated and represented on the head model. OptoNet provides visual brain connection to easily identify the cortical network, and there are various view options, as indicated in Fig. 2.

The head and cortex models can be loaded by the GUI button shown in Fig. 2(a). OptoNet allows 3-D rotations to enable visualization of every direction on the head. Additionally, it can set up numerous view options, such as the depiction of the points associated with the 10–20 system, camera light (camlight), interpolation (interp), depiction of axis (view axis), and the depiction of the mesh plot (view mesh) with the use of the checkbox on the GUI panel in Fig. 2(b). The fNIRS channels can be set up using the panel in Fig. 2(c) and can load a saved channel set using the panel in Fig. 2(d). The connectivity estimation method and threshold are established using the panel shown in Fig. 2(e). OptoNet provides not only PLV but also additional three methods, which are correlation,[29,30] coherence,[31] and frequency ratio.[32] Correlation is one of the most widely used methods to evaluate signal similarity in time domain. Coherence measures the phase similarity of two signals in the frequency domain, and the frequency ratio is a measure of frequency synchronization that is evaluated by frequency ratio. However, PLV was selected by the connectivity estimation method of this study, because it can simultaneously evaluate time–frequency synchronization between two signals. These provide the choice of automatic or manual thresholding. The autothresholding type is statistically evaluated by surrogate datasets, and it can be set up to acquire specific values from 0 to 1 when the manual-threshold is selected. Finally, the significant cortical connections, which were evaluated by surrogate datasets or have higher causality values than the setup threshold, are represented on the GUI. The estimation result of the functional causality can be automatically saved into MATLAB. mat files, which can be loaded in MATLAB at any time.

3 Experimental Results

This section introduces an example that demonstrates the utility of the OptoNet toolbox. The experimental task paradigm consisted of the finger tapping task combined with a rest control task. Seven subjects (24.1 ± 5.64 years, five males, two females, and right-handed) were recruited. All subjects were healthy with no brain injury, neurologic, or psychiatric disease profiles. Informed consent was obtained from all subjects. Using a block design, the fNIRS signal of the subjects was measured, where three activation trials were alternated while repetitive finger tapping was performed with the right hand, left hand, and simultaneously with the use of both hands, during a 20-s period. fNIRS data acquisition was performed with an fNIRS brain imaging system (NIRsPORT 8–8, NIRx Medizintechnik GmbH, Berlin, Germany). This instrument emitted LED light with wavelengths in the range of 760 and 850 nm with eight NIR sources, eight NIR detectors, and 20 fNIRS channels. The arrangements of the fNIRS channels and optodes are shown in Fig. 3. Figure 3(a) depicts the structure of the optodes that formed the fNIRS system with 20 channels, Fig. 3(b) presents the channel locations based on the use of the head model of OptoNet, and Fig. 3(c) shows the actual experimental fNIRS cap with the eight wired sources and eight detectors. The regions-of-interest of the finger tapping were selected within the primary motor cortex (M1) and the supplementary motor area (SMA).[45] The fNIRS channels in Fig. 3 cover the SMA and M1 of the left and right hemispheres, which are areas related to the finger tapping task.

To estimate the hemodynamic signals (HbO and HbR) and the brain activity map, data processing was performed using the NIRS–SPM software[14,39] in MATLAB. Two wavelengths (760 and 850 nm) of LED light were used for this experiment, and the DPFs were set to 6.2966 for the wavelength of 760 nm, and 5.23433 for the wavelength of 850 nm, as recommended in the user manual of NIRsPORT. To enhance the fNIRS signal, an HRF smoothing filter[44] was applied for preprocessing. A first-level of analysis used the preprocessed fNIRS data to obtain parameter images of individuals for contrasting the design (finger tapping task > rest control task). The brain activity images from all the subjects were entered into a second-level analysis group with one-sample t-test to confirm the statistically significant cortical activation area of the motor task ($p < 0.05$). The brain activation results of the finger tapping task are shown in Fig. 4. As can be observed in Fig. 4, the M1 of the left hemisphere was activated from the right-hand finger tapping task in Fig. 4(a). From the left-hand task in Fig. 4(b), the right M1 was strongly activated, and Fig. 4(c) shows the result of the tasks conducted with both hands indicating activities in M1 on both hemispheres. The results of the fNIRS cortical functional connection were estimated using Monte Carlo simulations with PLV.[33] The group analyses results of the

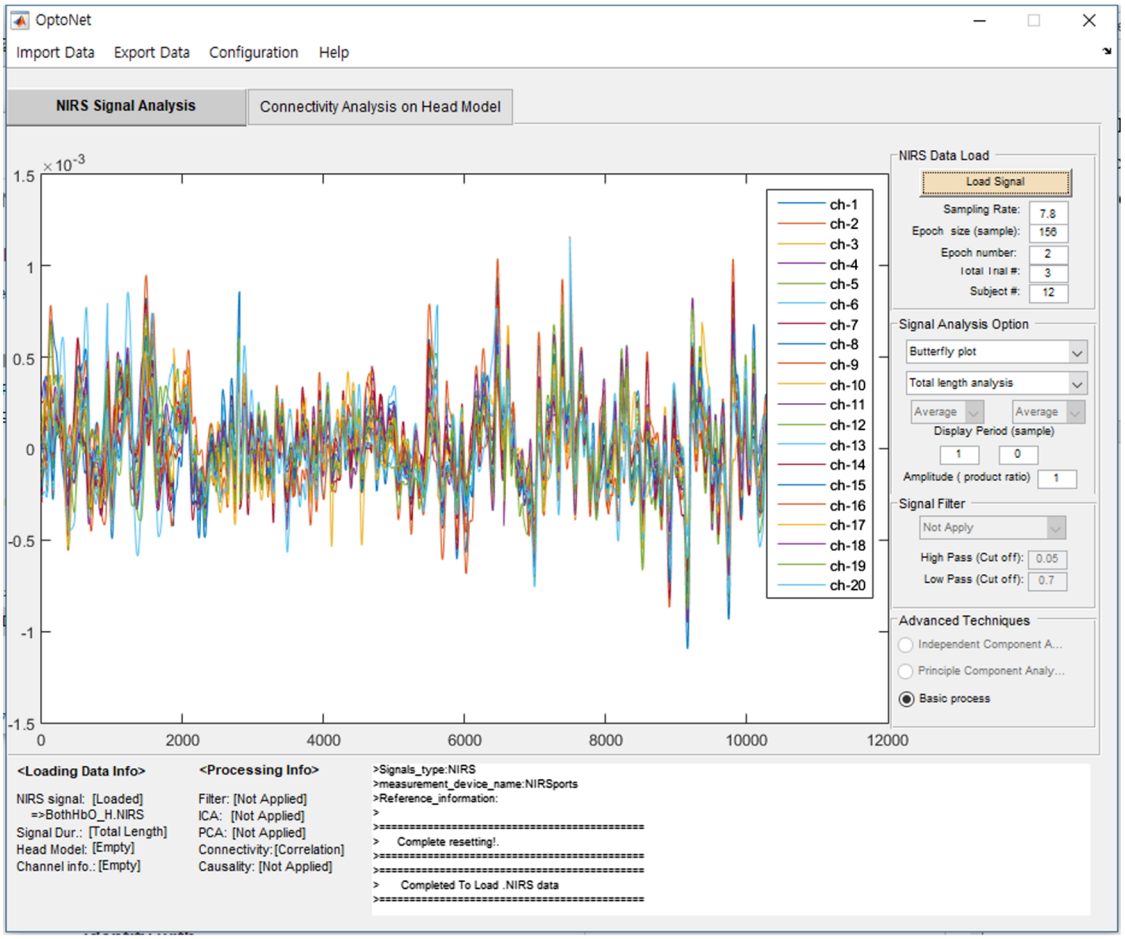

(a)

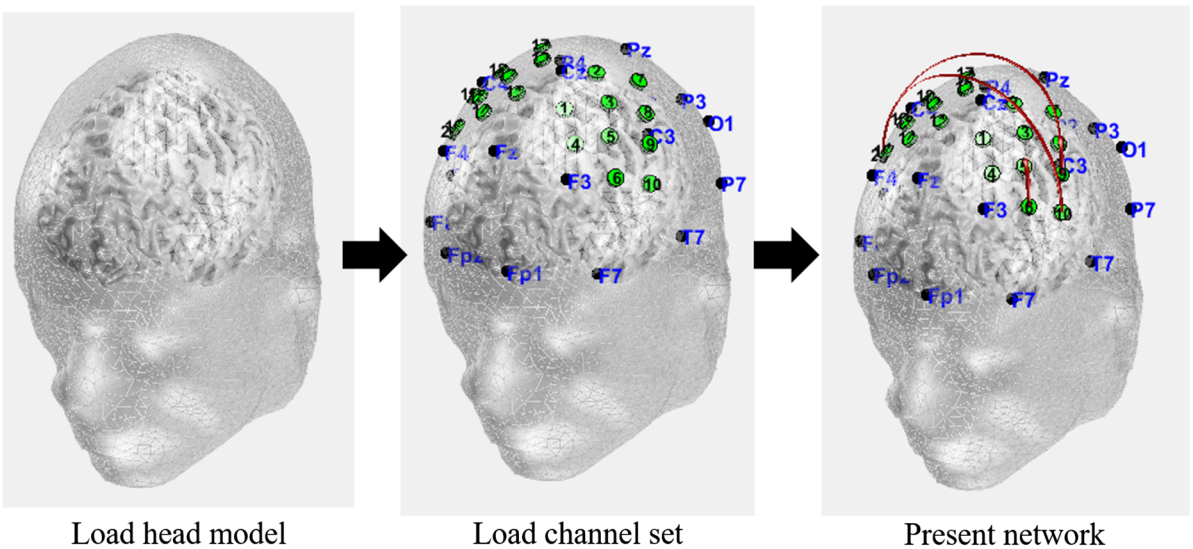

(b)

Fig. 1 Procedure of OptoNet toolbox: (a) GUI capture showing the loading of fNIRS data and (b) loaded head model, generation of an *f*NIRS channel set, and cortical network visualization. Example of OptoNet process is shown in Video 1 (MP4, 32.2 MB [URL: https://doi.org/10.1117/1.OE.59.6.061602.1]).

cortical connections were elicited with the use of OptoNet based on estimations with all trials, all epochs, and all subjects, as shown in Fig. 5. Figure 5(a) shows the functional connections at M1 of the left hemisphere following the right-hand finger-tapping task, and they are represented in the same regions of the detected brain activities shown in Fig. 4(a). In Fig. 5(b), the functional connection result of the left-hand shows the connections that are connected to a

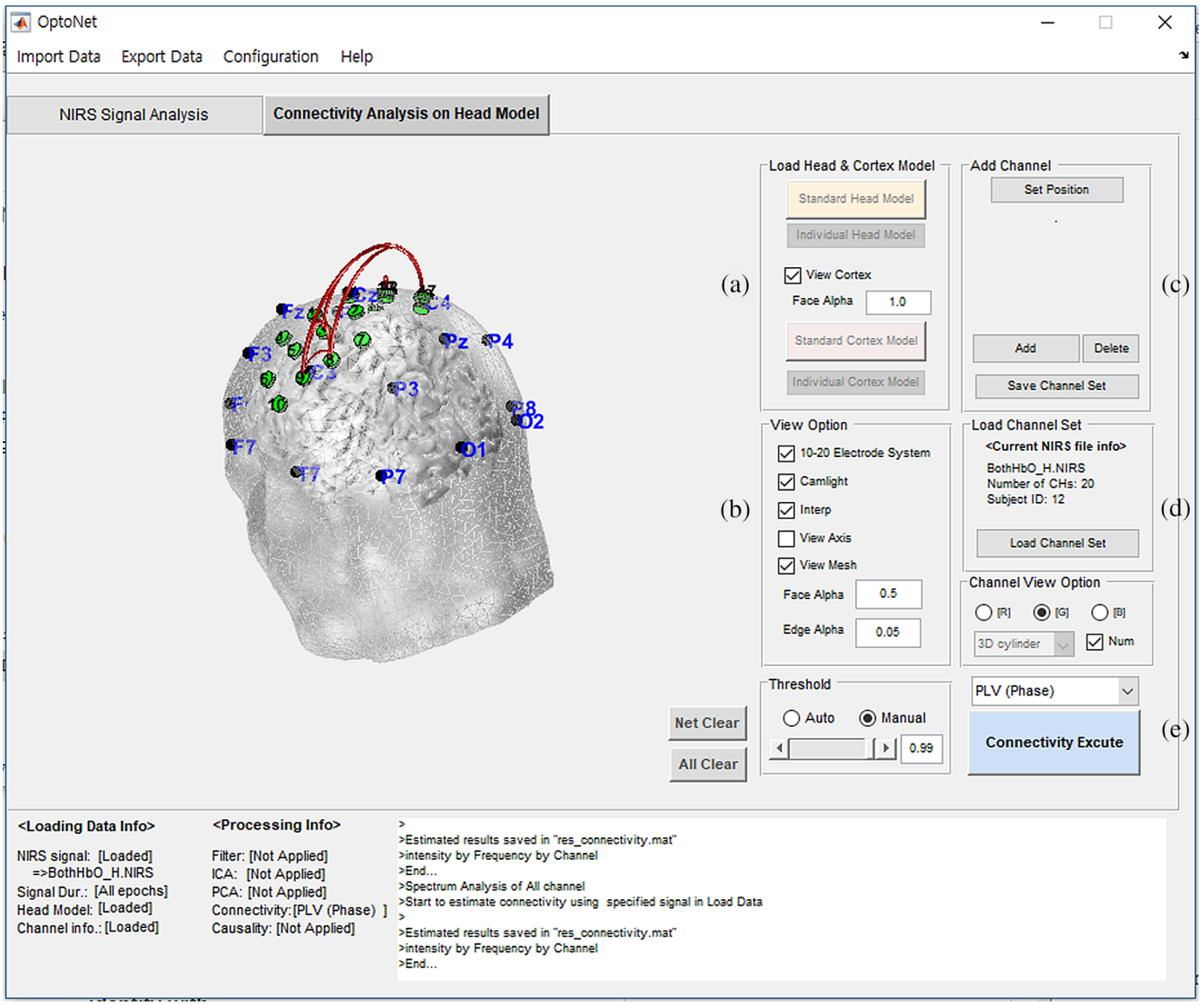

Fig. 2 Control panel in the OptoNet GUI.

larger region in the right hemisphere. Figure 5(c) shows the functional connection results following the execution of the finger-tapping task of both hands. The results show the functional connections at both sides of the M1 of the right and left hemisphere, where the connections are established on both sides of the brain.

4 Discussion

Functional brain network analyses of fNIRS have played an important role in recent fNIRS studies. Heretofore, most fNIRS studies focused on the hemodynamic activation elicited owing to the vasodilation. Given that fNIRS signals contain numerous artifacts, such as baseline drifts, measured noise, equipment noise, and motion artifacts, it is not easy to estimate a correct hemodynamic dataset. Further, it is very difficult to identify a hemodynamic response from a task that generates little motion. Therefore, the research focus needs to shift toward the description of how different brain areas interact with one another to understand the functional organization of the cortical network.

We have developed a MATLAB toolbox called OptoNet that can be used to analyze functional cortical networks for fNIRS. It is easy and simple to use for plotting fNIRS signals and functional cortical connections without anatomical information, such as 3-D MRI images and MNI co-ordinates. To demonstrate the performance of OptoNet, the well-known finger-tapping task experiment was conducted, and the brain activation function was mapped.[46–50] The task was performed with the right and left hands, as well as with both hands. Accordingly, the cortical brain activity results were represented pictorially and showed the well-known role of the hand movements in the opposite sides of the two cerebral hemispheres. However, the activation of the left-hemispheric areas was much smaller than the activation of the right areas. This is indicative of the fact that there is much stronger and wider activation from the left-hand movements than the right-hand, and it appears to be in accordance with efficient activities of the dominant hand, which represents a small area because it is using the brain efficiently and because it is used for the action.[51–53] However, the elicited outcomes cannot be clearly demonstrated based only on brain activation maps.

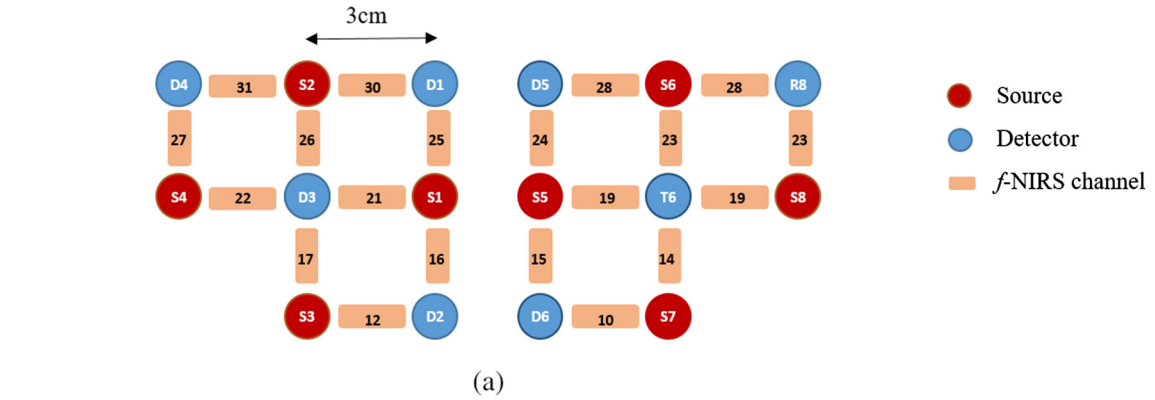

Fig. 3 *f*NIRS measuring information: (a) schematic diagram of the source and detector, (b) *f*NIRS channel locations on the head model, and (c) fNIRS cap with 8×8 wired optodes.

Although the brain areas that elicited significant connections were estimated to exist at similar locations to those associated with the brain activation maps, the functional brain network yielded connectivity differences between the right and left hemispheres. Figure 5(a) showed that the functional connections have a strong and close-set network in each other's fNIRS channels from the movement of the dominant hand. Further, the functional connections from the left-hand movement in Fig. 5(b) exhibit a weaker connection than the right-hand movements in Fig. 5(a). It can be seen in Fig. 5(c) that there are functional connections across the right- to left-hemisphere and strong and close-set connections can be

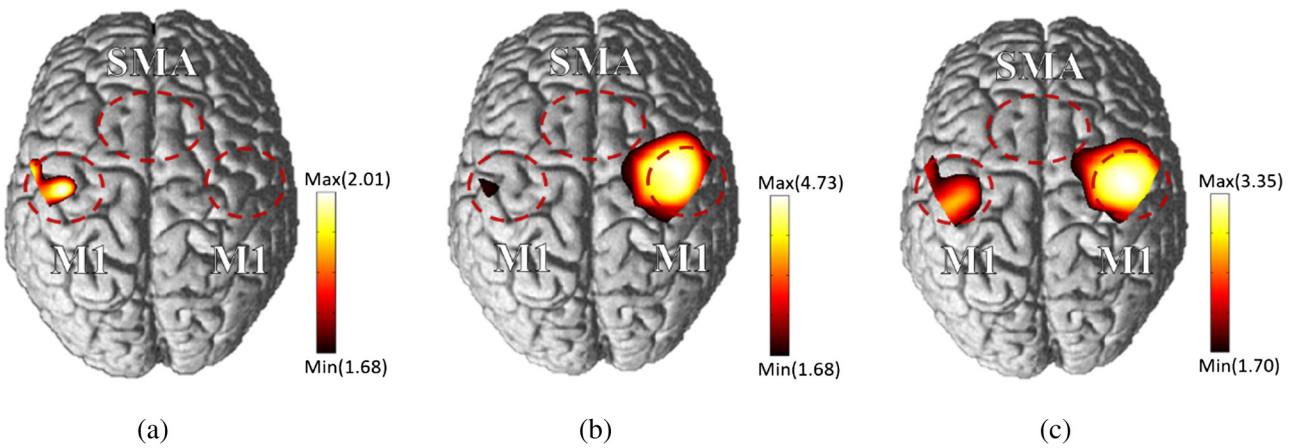

Fig. 4 Group analysis brain activity maps with the use of NIRS SPM ($p < 0.05$) elicited with (a) finger tapping tasks of the right hand, (b) the left hand, and (c) following the simultaneous tapping of both hands.

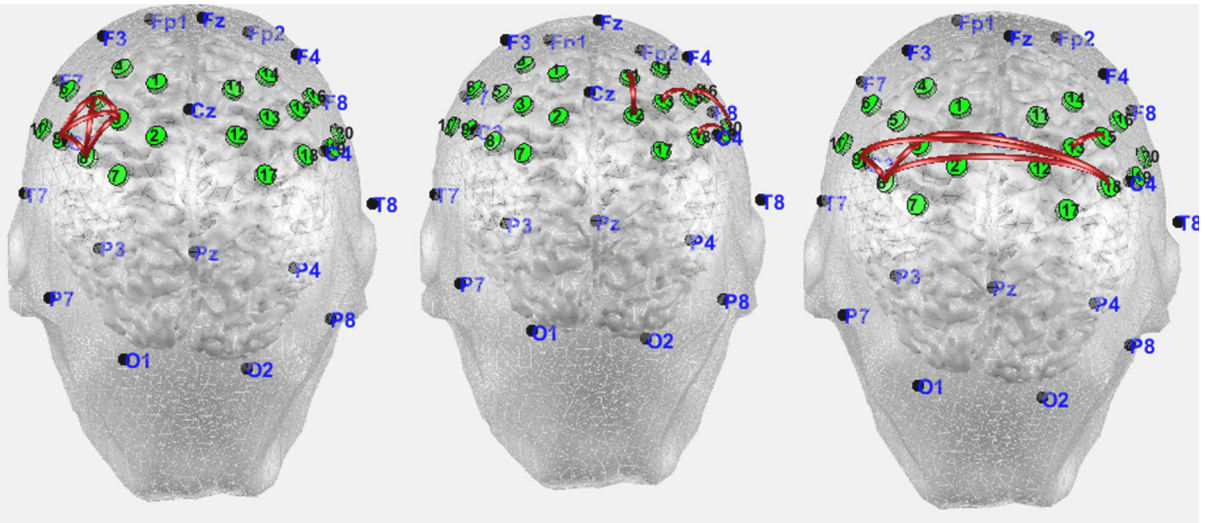

Fig. 5 Group analyses outcomes of cortical functional connections with the use of OptoNet ($p < 0.01$), elicited with the finger tapping tasks of (a) the right hand, (b) left hand, and (c) the simultaneous use of both hands.

found in the left-hemisphere. Therefore, OptoNet is a very powerful toolbox that can be used to estimate functional cortical connectivity, and it can help identify other information in the brain, which cannot be detected using conventional brain activation analyses.

5 Conclusions

In the present study, OptoNet was evaluated to estimate its strengths and to validate its performance for brain functional network analyses. We demonstrated the necessity and performance of OptoNet with the use of the basic experimental paradigm of fNIRS. Given that the technique of brain network analysis can be used for the understanding of neuroscience and neurological clinical studies, OptoNet has tremendous potential for use in brain cortical network research of fNIRS.

OptoNet can be downloaded for free from Ref. 54. The toolbox can be used for research and educational purposes. The user manual for OptoNet is included in the download page. We invite users to provide feedback for improving OptoNet on the website. We hope that our toolbox can contribute to the popularization of brain network analyses of cortical connectivity in the field of fNIRS research.

Acknowledgments

This work was supported by Dongseo University, "Dongseo Cluster Project" Research Fund of 2019 (Grant No. DSU-2019002).

References

1. A. Villringer and U. Dirnagl, "Coupling of brain activity and cerebral blood flow: basis of functional neuroimaging," *Cerebrovasc. Brain Metab. Rev.* **7**(3), 240–276 (1995).
2. M. Cope and D. T. Delpy, "System for long-term measurement of cerebral blood and tissue oxygenation on newborn infants by near infra-red transillumination," *Med. Biol. Eng. Comput.* **26**(3), 289–294 (1988).
3. Y. Hoshi, "Functional near-infrared optical imaging: utility and limitations in human brain mapping," *Psychophysiology* **40**(4), 511–520 (2003).
4. R. W. Homan, J. Herman, and P. Purdy, "Cerebral location of international 10–20 system electrode placement," *Electroencephalogr. Clin. Neurophysiol.* **66**(4), 376–382 (1987).
5. M. Okamoto et al., "Three-dimensional probabilistic anatomical cranio-cerebral correlation via the international 10–20 system oriented for transcranial functional brain mapping," *Neuroimage* **21**(1), 99–111 (2004).
6. T. Fekete et al., "The NIRS analysis package: noise reduction and statistical inference," *PloS One* **6**(9), e24322 (2011).
7. J. van Erp, F. Lotte, and M. Tangermann, "Brain-computer interfaces: beyond medical applications," *Computer* **45**(4), 26–34 (2012).
8. A. Kleinschmidt et al., "Simultaneous recording of cerebral blood oxygenation changes during human brain activation by magnetic resonance imaging and near-infrared spectroscopy," *J. Cereb. Blood Flow Metab.* **16**(5), 817–826 (1996).
9. D. A. Benaron et al., "Noninvasive functional imaging of human brain using light," *J. Cereb. Blood Flow Metab.* **20**(3), 469–477 (2000).
10. D. Boas et al., "Can the cerebral metabolic rate of oxygen be estimated with near-infrared spectroscopy?" *Phys. Med. Biol.* **48**(15), 2405–2418 (2003).
11. N. Fujiwara et al., "Evoked-cerebral blood oxygenation changes in false-negative activations in BOLD contrast functional MRI of patients with brain tumors," *Neuroimage* **21**(4), 1464–1471 (2004).
12. R. A. Shirvan, S. K. Setarehdan, and A. M. Nasrabadi, "A new approach to estimating the evoked hemodynamic response applied to dual channel functional near infrared spectroscopy," *Comput. Biol. Med.* **84**, 9–19 (2017).
13. W. Wei et al., "A near-infrared spectrometer based on novel grating light modulators," *Sensors* **9**(4), 3109–3121 (2009).
14. J. C. Ye et al., "NIRS-SPM: statistical parametric mapping for near-infrared spectroscopy," *Neuroimage* **44**(2), 428–447 (2009).
15. M. L. Schroeter et al., "Towards a standard analysis for functional near-infrared imaging," *NeuroImage* **21**(1), 283–290 (2004).
16. M. Plichta et al., "Model-based analysis of rapid event-related functional near-infrared spectroscopy (NIRS) data: a parametric validation study," *Neuroimage* **35**(2), 625–634 (2007).
17. P. H. Koh et al., "Functional optical signal analysis: a software tool for near-infrared spectroscopy data processing incorporating statistical parametric mapping," *J. Biomed. Opt.* **12**(6), 064010 (2007).
18. F. Aletti et al., "Deep and surface hemodynamic signal from functional time resolved transcranial near infrared spectroscopy compared to skin flowmotion," *Comput. Biol. Med.* **42**(3), 282–289 (2012).
19. K. E. Jang et al., "Wavelet minimum description length detrending for near-infrared spectroscopy," *J. Biomed. Opt.* **14**(3), 034004 (2009).
20. X. Cui, S. Bray, and A. L. Reiss, "Functional near infrared spectroscopy (NIRS) signal improvement based on negative correlation between oxygenated and deoxygenated hemoglobin dynamics," *Neuroimage* **49**(4), 3039–3046 (2010).
21. M. Izzetoglu et al., "Motion artifact cancellation in NIR spectroscopy using Wiener filtering," *IEEE Trans. Biomed. Eng.* **52**(5), 934–938 (2005).

22. G. Lee et al., "Cross-correlation between HbO and HbR as an effective feature of motion artifact in fNIRS signal," in *6th Int. Conf. Brain-Comput. Interface (BCI)*, pp. 1–3 (2018).
23. G. Lee et al., "fNIRS motion artifact correction for overground walking using entropy based unbalanced optode decision and wavelet regression neural network," in *IEEE Int. Conf. Multisensor Fusion and Integr. Intell. Syst. (MFI)*, pp. 186–193 (2017).
24. G. Lee et al., "Baseline drift detection index using wavelet transform analysis for fNIRS signal," in *5th Int. Winter Conf. Brain-Comput. Interface (BCI)*, pp. 73–76 (2017).
25. G. Lee et al., "Selective detrending using baseline drift detection index for task-dependant fNIRS signal," *Adv. Sci. Technol. Eng. Syst. J.* **2**(3), 1147–1151 (2017).
26. G. Lee et al., "Robust functional near infrared spectroscopy denoising using multiple wavelet shrinkage based on a hemodynamic response model," *J. Near Infrared Spectrosc.* **26**(2), 79–86 (2018).
27. G. Lee, S. Jin, and J. An, "Motion artifact correction of multi-measured functional near-infrared spectroscopy signals based on signal reconstruction using an artificial neural network," *Sensors* **18**(9), 2957 (2018).
28. Y.-J. Jung, K. H. Kim, and C.-H. Im, "Mathematical issues in the inference of causal interactions among multichannel neural signals," *J. Appl. Math.* **2012**, 1–14 (2012).
29. A. Aarabi, F. Wallois, and R. Grebe, "Does spatiotemporal synchronization of EEG change prior to absence seizures?" *Brain Res.* **1188**, 207–221 (2008).
30. G. Thut et al., "Rhythmic TMS causes local entrainment of natural oscillatory signatures," *Curr. Biol.* **21**(14), 1176–1185 (2011).
31. G. Varotto et al., "Spectral and coherence analysis of EEG during intermittent photic stimulation in patients with photosensitive epilepsy," *Int. J. Bioelectromagn.* **11**(4), 189–193 (2009).
32. I. Yilmaz, "Landslide susceptibility mapping using frequency ratio, logistic regression, artificial neural networks and their comparison: a case study from Kat landslides (Tokat—Turkey)," *Comput. Geosci.* **35**(6), 1125–1138 (2009).
33. J. P. Lachaux et al., "Measuring phase synchrony in brain signals," *Hum. Brain Mapp.* **8**(4), 194–208 (1999).
34. F. Mormann et al., "Mean phase coherence as a measure for phase synchronization and its application to the EEG of epilepsy patients," *Physica D* **144**(3-4), 358–369 (2000).
35. S. Baillet et al., "Combined MEG and EEG source imaging by minimization of mutual information," *IEEE Trans. Biomed. Eng.* **46**(5), 522–534 (1999).
36. J. Jeong, J. C. Gore, and B. S. Peterson, "Mutual information analysis of the EEG in patients with Alzheimer's disease," *Clin. Neurophysiol.* **112**(5), 827–835 (2001).
37. T. J. Huppert et al., "HomER: a review of time-series analysis methods for near-infrared spectroscopy of the brain," *Appl. Opt.* **48**(10), D280–D298 (2009).
38. D. Boas and J. Dubb, "HOMER," http://www.nmr.mgh.harvard.edu/PMI/resources/homer/home.htm (2005).
39. J. C. Ye, https://bispl.weebly.com/nirs-spm.html (2012).
40. A. F. Abdelnour and T. Huppert, "Real-time imaging of human brain function by near-infrared spectroscopy using an adaptive general linear model," *Neuroimage* **46**(1), 133–143 (2009).
41. A. Duncan et al., "Optical pathlength measurements on adult head, calf and forearm and the head of the newborn infant using phase resolved optical spectroscopy," *Phys. Med. Biol.* **40**(2), 295–304 (1995).
42. M. Essenpreis et al., "Wavelength dependence of the differential pathlength factor and the log slope in time-resolved tissue spectroscopy," in *Optical Imaging of Brain Function and Metabolism*, U. Dirnagl, A. Villringer, and K. M. Einhäupl, Eds., Advances in Experimental Medicine and Biology, Vol. **333**, pp. 9–20, Springer, Boston, Massachusetts (1993).
43. W. D. Penny et al., *Statistical Parametric Mapping: The Analysis of Functional Brain Images*, Academic Press, New York (2011).
44. K. J. Friston et al., "Event-related fMRI: characterizing differential responses," *Neuroimage* **7**(1), 30–40 (1998).
45. M. Dhamala et al., "Neural correlates of the complexity of rhythmic finger tapping," *Neuroimage* **20**(2), 918–926 (2003).
46. S. T. Witt, A. R. Laird, and M. E. Meyerand, "Functional neuroimaging correlates of finger-tapping task variations: an ALE meta-analysis," *Neuroimage* **42**(1), 343–356 (2008).
47. C. H. Moritz et al., "Whole-brain functional MR imaging activation from a finger-tapping task examined with independent component analysis," *Am. J. Neuroradiol.* **21**(9), 1629–1635 (2000).
48. V.-E. Gountouna et al., "Functional magnetic resonance imaging (fMRI) reproducibility and variance components across visits and scanning sites with a finger tapping task," *Neuroimage* **49**(1), 552–560 (2010).
49. C. A. Carroll et al., "Timing dysfunctions in schizophrenia as measured by a repetitive finger tapping task," *Brain Cognit.* **71**(3), 345–353 (2009).
50. J. E. Desmond et al., "Lobular patterns of cerebellar activation in verbal working-memory and finger-tapping tasks as revealed by functional MRI," *J. Neurosci.* **17**(24), 9675–9685 (1997).
51. S. T. Yang et al., "Dominant and subdominant hand exhibit different cortical activation patterns during tactile stimulation: an fNIRS study," in *6th Int. Conf. Brain-Comput. Interface (BCI)*, pp. 1–3 (2018).
52. P. S. Boggio et al., "Enhancement of non-dominant hand motor function by anodal transcranial direct current stimulation," *Neurosci. Lett.* **404**(1–2), 232–236 (2006).
53. L. Jäncke et al., "The effect of finger-movement speed of the dominant and the subdominant hand on cerebellar activation: a functional magnetic resonance imaging study," *Neuroimage* **9**(5), 497–507 (1999).
54. Y. J. Jung, https://sites.google.com/site/dsucore/free/optonet (2019).

Gihyoun Lee is a postdoctoral researcher at Samsung Medical Center. He joined the Department of Physical and Rehabilitation Medicine, Center for Prevention and Rehabilitation, Heart Vascular Stroke Institute, in March 2019. He obtained his PhD, MS, and BS degrees from KNU in 2009, 2012, and 2016, respectively. His research interests are brain network analysis, neural networks, artificial intelligence, machine learning, brain signal processing, and brain activation mapping.

Ji-Su Park earned his PhD in the Department of Rehabilitation Science from Inje University, Gimhae, Republic of Korea, in 2018 and is now a research professor in the Advanced Human Resource Development Project Group for Health Care in Aging Friendly Industry at Dongseo University. His research interests brain stimulation, dysphagia, and therapeutic exercise for stroke.

Young-Jin Jung has completed his PhD from Yonsei University, and he worked at Hanyang University as a research assistant professor (2011). In 2012, he worked at the Engineering Center at Florida International University (FIU) as a postdoc, and then he was promoted to assistant professor at the College of Nursing and Health Science FIU in USA (2014–2015). He is now an assistant professor at the Department of Radiological Science at Dongseo University (Republic of Korea). His current research interest includes computational radiological engineering, especially signal and imaging processing and reconstruction.